Journal of the Ceramic Society of Japan 121 [7] 539-543 2013 Special Article
The 67th CerSJ Awards for Advancements in Ceramic Science and Technology: Review

Proton conduction in glasses prepared via sol–gel and melting techniques

Yusuke DAIKO†

Graduate school of Engineering, Nagoya Institute of Technology, Gokiso-cho, Showa-ku, Nagoya 466–8555, Japan

Phosphosilicate glasses were prepared using both sol–gel and conventional melting methods, and proton conductivity of these glasses was investigated. Glasses prepared by sol–gel method are porous, and proton conductivity increases significantly by absorption of water. The pore structure, especially pore size, is a crucial factor in order to obtain high proton conductivity in wide temperature/humidity ranges. On the other hand, in the case of glasses prepared via conventional melting method, proton incorporation into the glasses as well as decreasing alkali cation conductivity by utilizing the mixed-alkali effect are indispensable. Proton conduction mechanisms in these glasses are discussed.

Key-words : Proton conduction, Nanopore, Confinement effect, Proton incorporation, Mixed-alkali effect

[Received April 22, 2013; Accepted May 22, 2013]

1. Introduction

Solid electrolytes with high H^+ or O^{2-} ions conductivities have attracted considerable attention because of their potential applications as gas sensors and fuel cells.[1),2)] Polymer electrolyte fuel cells (PEFCs) using H^+ conducting polymer membranes (e.g., Nafion®, operating below 100°C),[3),4)] and solid oxide fuel cells (SOFCs) using O^{2-} conducting inorganic electrolytes[5)–7)] (e.g., yttrium-stabilized ZrO_2, operating around 800°C) have been offered commercially. Although perfluorosulfonate ionomers exhibit high proton conductivity of ≈0.1 S/cm, the conductivity decreases around 100°C, because of their inability to contain water. Nafion® films are susceptible to deformation based on their repetition of the adsorption and desorption of water.[8),9)] In addition, their thermal and chemical degradations around 100°C would limit their applications. On the other hand, the operation temperature of ≈800°C for SOFC is too high, and a heat-stable framework is required for SOFCs, leading to increase the fabrication cost.

Polymer electrolytes show a high proton conductivity when they absorb water molecules, and the state of the water including hydroxyl groups has been considered as a crucial factor for high proton conductivity. The protons in glasses exist mainly as OH groups. From the 1950's, studies about the amount of water,[10)] solubility of water under ambient or high pressure conditions,[11)–14)] bonding state, hydrogen bond for glass or glass-melt have been performed using Fourier transform infrared (FTIR), Raman and nuclear magnetic resonance (NMR) spectroscopies.[15)–20)] The states of the OH groups in glasses were first studied extensively by Scholze, for silicate glasses.[21)] It is noteworthy that there are only a few protons inside melting-glasses. For typical oxide glasses, the melting temperatures of glasses are higher than 1000°C, and the OH groups evaporate during the melting procedure. Also, the Pauling electronegativity of H is 2.1, which is much higher than that of Na (0.9). Therefore, $-O^-$ and H^+ ionic pairs are strongly bonded to each other, leading to a high dissociation energy of the proton. It has therefore generally been accepted that protons in oxide glasses are much less mobile than other cations such as alkali-metal or Ag^+ ions; for example, Doremus estimated that in silicate glass the mobility of Na^+ ions is 10^4 times that of protons.[22)–24)]

Unlike melting-glasses, by utilizing a sol–gel method, porous glasses with a large amount of water molecules can be obtained. Stable inorganic materials with high conductivity over a wide temperature range, if developed, would extend beyond the limitation of PEFC and SOFC. In this paper, proton conduction in glasses prepared via sol–gel and melting techniques is discussed.

2. Proton conduction in sol–gel-derived nanoporous glasses

Porous phosphosilicate $5P_2O_5$–$95SiO_2$ (mol%) glasses were prepared by the sol–gel method.[25),26)] The synthesis of these solutions was done at room temperature. The detailed preparation procedures are given in elsewhere.[27)] The obtained solutions were clear and were left for several weeks to form stiff gels in Petri dishes. The dried gels were heated at 50°C/h to 600–700°C and held at that temperature for 5 h, and the thickness of the obtained glass plates was about 0.3 mm.

The P^{5+} and Si^{4+} ion contents in glasses were determined by inductivity coupled plasma spectroscopy. The powder samples were dissolved in a KOH solution. Specific surface area, pore volume and pore size distribution were measured using a Quantachrome NOVA 1000 nitrogen gas sorption analyzer. All the samples were heated in advance at 250°C in a vacuum in order to remove the adsorbed water remaining in the pores. The pore size distribution was determined by the Barrett–Joyner–Halenda (BJH) method.[28)]

The electrical conductivities for glasses, measured without exposure to an ambient atmosphere after the heat treatment, are lower than $\approx 1 \times 10^{-7}$ S/cm at room temperature. When the glasses are exposed to ambient air, they absorb water. Correspondingly, the conductivity increases and reaches a constant value within several tens of minutes. The conductivity is not unconditionally determined by the pore volume.

† Corresponding author: Y. Daiko; E-mail: daiko.yusuke@nitech.ac.jp

DOI http://dx.doi.org/10.2109/jcersj2.121.539

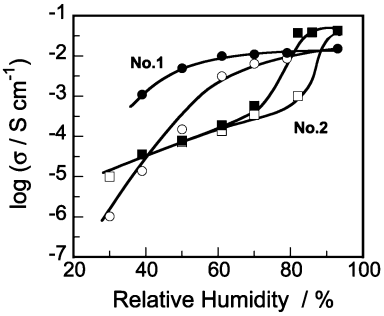

Fig. 1. Relative humidity dependences of the proton conductivity, measured at 30°C, for samples No. 1 and No. 2. Open and closed marks indicate the adsorption and desorption branch of humidity, respectively.

Table 1. Specific surface area, pore volume, average pore radius and molar ratio of P and Si atoms of glasses

Sample No.	P/Si	Pore volume (cm^3/g)	Specific surface area (m^2/g)	Average pore radius (nm)
1	0.058	0.44	584	1.5
2	0.155	0.52	130	8.1

The conductivities for two typical porous glasses, measured after exposure to ambient humidity for long period at 30°C, are plotted in **Fig. 1** as a function of the relative humidity. The pore structures (pore volume, specific surface area and pore radius) and P/Si compositions are summarized in **Table 1**. The conductivities were measured upon increasing the relative humidity from 30 to 90%, followed by decreasing it from 90 to 30%. It is evident that the conductivity increases with increasing relative humidity, however the humidity dependence is substantially different between the two samples. In the sample **No. 1**, the conductivity is $\approx 1 \times 10^{-6}$ S/cm at 30%RH, and rapidly increases with increasing humidity, reaching a constant value of $\approx 1 \times 10^{-2}$ S/cm at the humidity above 70%RH. Note in Fig. 1 that sample **No. 1** maintains high conductivities of $\sim 10^{-2}$ S/cm during decreasing humidity, though gradually decreasing at a humidity below 50%RH. This result indicates that the glass, exposed once to high humidity, holds the water in its pores and exhibits a high conductivity irrespective of the humidity change. This finding is important for the practical application of the sol–gel-derived porous glasses, because they allow a simple water management for fuel cell operation, consequently resulting in a significant decrease in the operating cost of fuel cell. On the other hand, the sample **No. 2** exhibits a gradual increase in the conductivity with increasing humidity up to 80%, at which the conductivity rapidly increases and reaches $\approx 5 \times 10^{-2}$ S/cm. The conductivity of sample **No. 2** reversibly changes with the changed humidity.

At high relative humidity regions, the glass with larger pores shows higher conductivity. Similar result was obtained for porous SiO_2 glasses. By utilizing pulse field gradient NMR technique,[29),30)] it was found that the proton mobility changes clearly with the pore size; *e.g*, the proton mobility of 2-nm (pore radius) and 1-nm SiO_2 glasses were 2.7×10^{-4} and 1.7×10^{-4} cm^2/V s, respectively.[31)]

The proton motion in the porous glasses was investigated based on the measurement of the relaxation dynamics using ^{1}H NMR spectroscopy.[32)–34)] The spin–lattice relaxation time was measured by using the standard inversion recovery technique. It was found that the relaxation time decreases for water molecules adsorbed in the glasses with small pores. The deviations of the relaxation time from that of the free water ($T_1 = 2.7$ s) are plotted

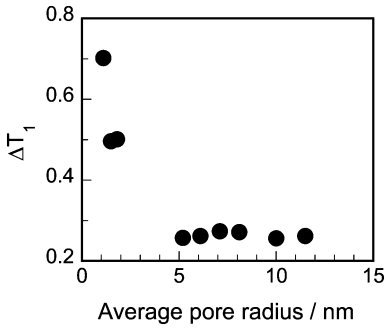

Fig. 2. Relationship between the spin–lattice relaxation time of proton and average pore radius. The values in the ordinate are shown as the deviation from the relaxation time of free water.

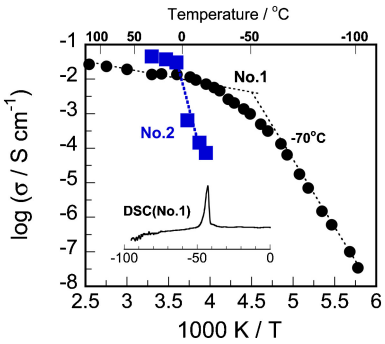

Fig. 3. Temperature dependence of proton conductivity of samples No. 1 and 2.

in **Fig. 2** as a function of the pore size. The deviation becomes significant below 5 nm in pore radius (so-called a confinement effect). Sample **No. 1** has pores with an average size of 1.5 nm, and the motion of the water molecules is restricted by the small-sized pores, resulting into decrease the proton mobility.

It is known that water in nanopores does not freeze around 0°C. **Figure 3** shows the conductivity dependence on temperature for samples **No. 1** and **2**. The conductivities were measured in constant humidity of 90%RH, except for the temperature below 0°C. For conductivity measurement below 0°C, the sample was kept at 90%RH and 5°C and then the temperature was decreased to below 0°C, at which the conductivities were measured.[35)] Note that the conductivities for sample **No. 1** are well represented by one Arrhenius equation down to around −40°C, at which the conductivity deviates from the linear relation to follow a different line with a large activation energy. The freezing temperature of water in sample **No. 1** was determined by the differential scanning calorimetric experiment, which was −40°C (inset of Fig. 3), consistent with the discontinuous points observed in the conductivity-temperature curves. Around −100°C, the Cole–Cole plot was not obtained because of its very high resistance. On the other hand, the conductivity of sample **No. 2** abruptly decreases around 0°C. The water molecules confined in the small-sized pores are limited in motion and the freezing temperature decreased as the pore size decreases.[36)–38)] The high activation energy for proton conduction in the temperature range below the freezing point indicates that the solid water molecules do not work to accelerate the proton hopping.

Figure 4 shows the ^{1}H combined rotation and multiple pulse spectroscopy (CRAMPS)[39)] spectra measured at various temperatures down to −110°C. The spectra were measured upon decreasing temperature from 20 down to −110°C. A single peak

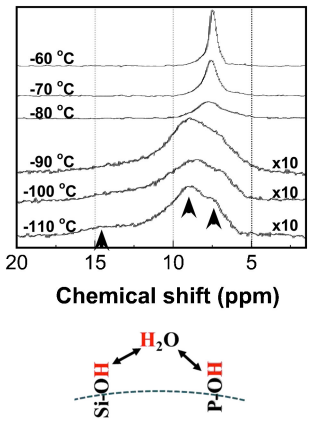

Fig. 4. ^{1}H CRAMPS spectra recorded at 200 MHz with a BR-24 pulse sequence at various temperatures for $5P_2O_5{\cdot}95SiO_2$ (mol %) glass. Arrows indicate the deconvoluted-peak positions.

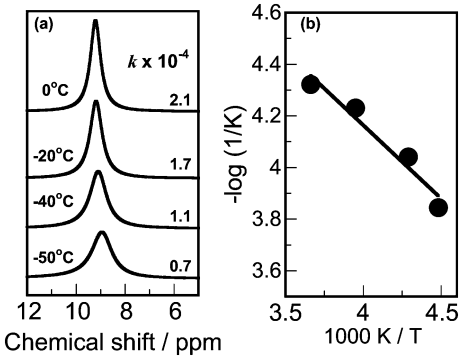

Fig. 5. (a) ^{1}H NMR spectra and the calculated k values, and (b) Arrhenius plot of the k from 0°C down to −50°C.

was observed from room temperature to around −70°C, and then the peak width became broad as the temperature decreases. Note that the sample at −90°C has broaden bands peaking at ≈7, 9 and 14 ppm, which are assigned to the protons of Si–OH, water molecules and P–OH, respectively. These NMR features strongly suggest that no proton exchange is taken place between the hydroxyl and the absorbed water molecules at −90°C or below.

The rate constant k for the proton exchange between P–OH, Si–OH and water molecules was calculated from the line width of NMR spectra, and results are shown in **Fig. 5**(a). The activation energy for the proton exchange was 10 kJ/mol [Fig. 5(b)], which is in good agreement with the activation energy for the proton hopping calculated from the conductivity data.

Unlike the commercially available polymer electrolyte, the glasses having small pores exhibit high conductivities even at temperatures below 0°C, and the controlling pore structure, especially pore size is quite necessary to manage the water.

3. Proton conduction in melting glasses

Although perfluorosulfonate ionomers (e.g. Nafion®) or sol–gel-derived porous glasses exhibit high proton conductivity, their industrial applications are limited by their low operation temperatures (<100°C). Fuel cell operation higher than 100°C in dry conditions is desired to increase the total efficiency, CO tolerance of Pt electrodes, increase the electrode reaction rate, and simplify system integration.[40)–42)] This has promoted a great interest in developing a new electrolyte with high proton or oxygen conductivity at intermediate temperature (300–500°C).

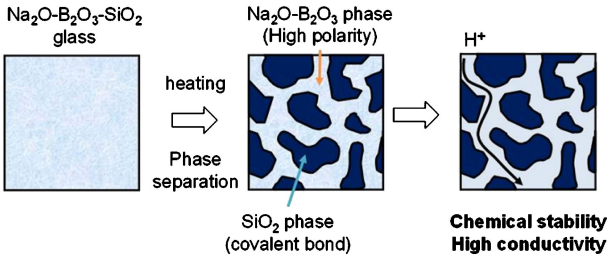

Fig. 6. Schematic illustration of the spinodal type phase separation of borosilicate and phosphosilicate glasses.

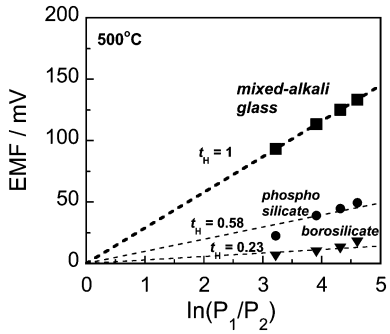

Fig. 7. Relationship between the hydrogen partial pressure (P_1/P_2) and electromotive force (EMF) of spinodal glasses at 500°C. The symbols in the figure are for the following glasses: black triangle, B $9.4Na_2O{\cdot}25.4B_2O_3{\cdot}65.2SiO_2$ (mol %) doped with 3% of P_2O_5; black circle, $15Na_2O{\cdot}35P_2O_5{\cdot}50SiO_2$ (mol %); black square, $7.5Na_2O{\cdot}7.5K_2O{\cdot}35P_2O_5{\cdot}50SiO_2$ (mol %).

Borosilicate and phosphosilicate glasses show typical spinodal-type phase separation by heating around those glass transition temperatures. As shown in **Fig. 6**, the ionic phase after the phase separation of glasses and the ionic channel of polymer electrolyte are similar, and it was reported that ionic conductivity increases after the phase separation.[43)] It was anticipated that a high proton conducting glasses can be obtained by utilizing the spinodal-type phase separation.

Borosilicate and phosphosilicate glasses were prepared using a conventional melting method. All glasses were X-ray amorphous. The proton transport number (t_H) of the glasses were estimated using a hydrogen concentration cell, and the relationship between electromotive force (EMF) and hydrogen partial pressures was measured (**Fig. 7**). The borosilicate glass ($9.4Na_2O{\cdot}25.4B_2O_3{\cdot}65.2SiO_2$ mol %) had $t_H \approx 0$, which indicates that few protons migrate in this glass. By contrast, when P_2O_5 (amount-of-substance fraction 3 mol %) was added to the borosilicate glass, the t_H was 0.23 at 500°C. Furthermore, the t_H of the phosphosilicate glass[44)] ($15Na_2O{\cdot}35P_2O_5{\cdot}50SiO_2$) increased up to 0.58 at the same temperature. However, in these borosilicate and phosphosilicate glasses, Na^+ ions migrated in addition to the protons, and these glasses were not applied as fuel cell electrolytes.

The pronounced changes in properties resulting from the addition of a second alkali oxide to a glass have been called the mixed-alkali effect.[45)–47)] The mixed-alkali effect refers to the large reduction of two to five orders of magnitude in the electrical conductivity that occurs when two or more alkali oxides are mixed. To decrease the mobility of Na^+ ions, a mixed-alkali glass with both sodium and potassium ions was prepared. It is immediately apparent in **Fig. 7** that the t_H of the mixed-alkali glass is increased to approximately 1.0. The data also suggests that the transport of protons is independent from that of alkali ions.

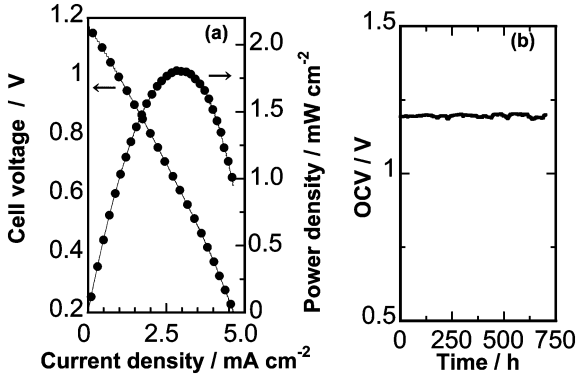

Fig. 8. (a) Fuel cell performances, and (b) durability test under the OCV condition using pure hydrogen and oxygen gasses for the mixed-alkali glass at 500°C.

Fuel cell performances were measured using the mixed-alkali glass, and the result is shown in **Fig. 8**(a). The anode and cathode electrodes used were Ni and $Ba_{0.5}Sr_{0.5}Fe_{0.2}Co_{0.8}O_3$,[48] respectively. Dry hydrogen (anode) and oxygen (cathode) gasses were supplied. The open-circuit voltage (OCV) of the mixed-alkali glass was ≈1.15 V. This value is much higher than that typically observed in polymer-based fuel cells (0.9–1.0 V). The result of lifetime measurement under the OCV condition is shown in Fig. 8(b). For the lifetime measurement, sputtered Pt electrodes were used. Note that the OCV remains unchanged and no degradation was observed for at least ≈750 h. This suggests the phosphosilicate glass with spinodal type phase separation is electrochemically/thermally stable around 500°C.

Similar to the typical oxide glasses, this mixed-alkali glass has few OH groups at the as-depo condition. To understand proton conduction mechanism under the fuel cell condition, an in-situ FTIR measurement was performed. CaF with 20 mm in diameter was used for IR window. Detailed experimental condition was described in elsewhere.[49]

The H_2 molecule reacts at the Pt anode side as follows;

$$H_2 \rightarrow 2H^+ + 2e^-$$

IR beam went through between the electrodes. Glass sample was heated at 300°C by using a micro-heater with a *k*-type thermo couple. Proton (OH groups) concentration during the pseudo-fuel cell operation was monitored by using the handmade in-situ FTIR equipment. **Figure 9**(a) shows FTIR spectra at 2700–3200 cm^{-1} region. Relationship between *Δabs*. (at 2900 and 3400 cm^{-1}) and the voltage-apply-time is shown in Fig. 9(b). The absorbance at 4000 cm^{-1} is also plotted as background because there is no absorption band for the glass at that wavenumber. The *Δabs* is denoted as follows;

$$\Delta abs = abs(\mathrm{t}) - abs(\mathrm{initial})$$

where *abs*(t) is the absorbance after applying 1 V for *t* minutes, and *abs*(initial) is the absorbance before applying 1 V. Note that OH groups observed at 2900 cm^{-1} increase gradually after applying 1 V, and then the value of *Δabs* seems to reach a constant value. It is evident that protons dissociated from H_2 gas at the Pt electrode can infiltrate into the phosphosilicate glass, resulting into increase the OH groups. Interestingly, no significant changes in absorbance were observed around 3400 cm^{-1} during the same measurement. The absorption band observed around 2900 cm^{-1} is assigned to OH stretching mode of P–OH groups,[50] whereas that observed around 3400 cm^{-1} is assigned to OH stretching mode of H_2O. It is clear from the in-situ FTIR results that protons infiltrated into the glass exist as P–OH groups. The non-bridging oxygen P=Ö (¨ indicates an unshared electron pair) may work as an acceptor site for the proton.

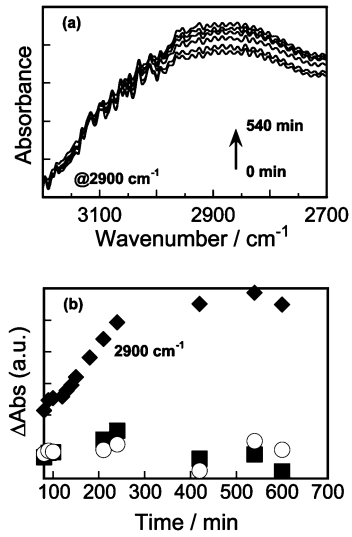

Fig. 9. (a) The results of in-situ FTIR measurements with voltage apply time up to 540 min, and (b) relationship between *Δabs* and the voltage applying time (◆; at 2900 cm^{-1}, ■; at 3400 cm^{-1}, ○; at 4000 cm^{-1}).

Table 2. The resistance of the mixed-alkali glass

Cell setup	Resistance (kΩ)
(100% H_2) Pt |glass| Pr (1% H_2–99% Ar)	2.6
(100% Ar) Pt |glass| Pr (100% Ar)	28

The electrochemical potential difference between Pt electrodes is also generated by using hydrogen concentration cell. Likewise the cell setup for the measurement of t_H, 100% of H_2 gas was exposed to a side of the glass and 1% H_2 (99% Ar) was exposed to the other side (**Table 2**). Pure Ar gas was also used as reference. It is interesting that the electrical resistance measured under hydrogen atmosphere was approximately one order of magnitude lower (2.6 kΩ) than that measured under Ar (28 kΩ). This result indicates that the main carrier is proton in the hydrogen concentration cell. As shown by FTIR results, the conductive ion carriers increase owing to the proton incorporation, resulting into decrease the resistance.

4. Conclusion

Proton conduction mechanism of glasses prepared via sol–gel and conventional melting methods are reviewed. Sol–gel-derived glasses are porous, and proton conductivity of these glasses increases by absorption of water. The dynamics of water molecules absorbed in nanopores are significantly restricted, especially less than 5 nm in pore radius, and proton mobility decreases with decreasing pore size. On the other hand, at sub-zero temperature region, porous glasses with ≈1 nm pores (radius) show relatively high proton conductivities down to −100°C. Such low-temperature proton conduction does not observe for polymer electrolytes.

Glasses prepared by melting method show very low proton conductivity because of their low carrier-density. Fourier-transform infrared (FTIR) measurements showed that protons dissociated from H_2 gas at the Pt electrodes incorporate into the glasses, and the proton conductivity increases as a result of an increase in the carrier (proton) concentration. Although the

maximum power density of the fuel cell is not large at present, the OCV of ≈1.1 V was successfully obtained at 500°C. Glass electrolytes have various advantages such as chemical and thermal stabilities, good formability, and low fabrication costs, and are promising candidates as electrolytes for intermediate-temperature fuel-cells.

Acknowledgement The author, Y. Daiko, is deeply grateful to Dr. M. Nogami and Dr. T. Kasuga (*Nagoya Inst. Tech.*), Dr. T. Yazawa and Dr. A. Mineshige (*Univ. Hyogo*), Dr. T. Minami (Osaka Prefecture Univ.), Dr. A. Matsuda and Dr. H. Muto (*Toyohashi Univ. Technol.*) and Dr. K. Katagri (*Hiroshima Univ.*) for their kind support and fruitful discussions. Advisers and colleagues of the author's researches, especially the students of Yazawa-lab, are also all very much appreciated. The works described in this paper were partially supported by the Ministry of Education, Culture, Sports, Science and Technology (MEXT) of Japan [Grant-in-Aid for Young Scientists (*Young A*), No. 23686095] and by Adaptable and Seamless Technology Transfer Program (A-STEP, JST no. AS221Z03900C).

References

1) C. H.-Wirguin, *J. Membr. Sci.*, 120, 1–33 (1996).
2) B. C. H. Steele and A. Heinzel, *Nature*, 414, 345–352 (2001).
3) K. A. Mauritz and R. B. Moore, *Chem. Rev.*, 104, 4535–4585 (2004).
4) C. H.-Wirguin, *J. Membr. Sci.*, 120, 1–33 (1996).
5) A. J. Jacobson, *Chem. Mater.*, 22, 660–674 (2010).
6) A. F. Sammells, *Solid State Ionics*, 52, 111–123 (1992).
7) J. W. Fergus, *J. Power Sources*, 162, 30–40 (2006).
8) B. Smitha, S. Sridhar and A. A. Khan, *J. Membr. Sci.*, 259, 10–26 (2005).
9) J. Wu, X. Yuan, J. J. Martin, H. Wang, J. Zhang, J. Shen, S. Wu and W. Merida, *J. Power Sources*, 184, 104–119 (2008).
10) E. Stolper, *Contrib. Mineral. Petrol.*, 81, 1–17 (1982).
11) C. R. Kurkjian and L. E. Russell, *J. Soc. Glass Technol.*, 42, 130–144 (1958).
12) J. W. Tomlinson, *J. Soc. Glass Technol.*, 40, 25–31 (1956).
13) J. R. Sweet and W. B. White, *Phys. Chem. Glasses*, 10, 246–251 (1969).
14) G. P. Crlova, *Int. Geol. Rev.*, 6, 254–258 (1964).
15) P. F. Mcmillan and R. L. Remmele, *Am. Mineral.*, 71, 772–778 (1986).
16) A. D. Pearson, G. A. Pasteur and W. R. Northover, *J. Mater. Sci.*, 14, 869–872 (1979).
17) K. Nakamoto, M. Margoshes and R. E. Rundle, *J. Am. Chem. Soc.*, 77, 6480–6486 (1955).
18) P. F. Mcmillan, S. Jakobsson, J. R. Holloway and L. A. Siver, *Geochim. Cosmochim. Acta*, 47, 1937–1943 (1983).
19) R. F. Bartholomew and J. W. H. Schreurs, *J. Non-cryst. Solids*, 38&39, 679–684 (1980).
20) J. Stone and G. E. Walrafen, *J. Chem. Phys.*, 76, 1712–1722 (1982).
21) H. Scholze, *Glastech. Chem. Ber.*, 32, 142 (1959) (ISSN: 0017-1085).
22) F. M. Ernsberger, *Phys. Chem. Glasses*, 21, 146–149 (1979).
23) F. M. Ernsberger, *J. Non-Cryst. Solid*, 38&39, 557–561 (1980).
24) R. H. Doremus, *J. Electrochem. Soc.*, 115, 181–186 (1968).
25) M. Nogami, K. Miyamura and Y. Abe, *J. Electrochem. Soc.*, 144, 2175–2178 (1997).
26) M. Nogami, R. Nagao, C. Wong, T. Kasuga and T. Hayakawa, *J. Phys. Chem. B*, 102, 5772–5775 (1998).
27) Y. Daiko, T. Kasuga and M. Nogami, *Chem. Mater.*, 14, 4624–4627 (2002).
28) E. P. Barrett, L. G. Joyner and P. P. Halenda, *J. Am. Chem. Soc.*, 73, 373–380 (1951).
29) E. O. Stejkal and J. E. Tanner, *J. Chem. Phys.*, 42, 288–292 (1965).
30) J. Kida and H. Uedaira, *J. Magn. Reson.*, 27, 253–259 (1977).
31) Y. Daiko, T. Kasuga and M. Nogami, *Micropo. Mesopo. Mater.*, 69, 149–155 (2004).
32) N. Bloembergen, E. M. Purcell and R. V. Pound, *Phys. Rev.*, 73, 679–712 (1948).
33) C. E. Bronnimann, R. C. Zeigler and G. E. Maciel, *J. Am. Chem. Soc.*, 110, 2023–2026 (1988).
34) J. H. Simpson and H. Y. Carr, *Phys. Rev.*, 111, 1201–1202 (1976).
35) Y. Daiko, T. Akai, T. Kasuga and M. Nogami, *J. Ceram. Soc. Japan*, 109, 815–817 (2001).
36) G. Hummer, J. C. Rasaiah and J. P. Noworyta, *Nature*, 414, 188–190 (2001).
37) Y. Maniwa, H. Kataura, M. Abe, S. Suzuki, Y. Achiba, H. Kira and K. Matsuda, *J. Phys. Soc. Jpn.*, 71, 2863–2866 (2002).
38) H. K. Christenson, *J. Phys.: Condens. Matter*, 13, R95–R133 (2001).
39) R. K. Harris, P. Jackson, L. H. Merwin, B. J. Say and G. Hägele, *J. Chem. Soc., Faraday Trans.*, 1, 3649–3672 (1988).
40) K. D. Kreuer, *Solid State Ionics*, 97, 1–15 (1997).
41) M. Nagao, A. Takeuchi, P. Heo, T. Hibino, M. Sano and A. Tomita, *Electrochem. Solid-State Lett.*, 9, A105–A109 (2006).
42) D. Pergolesi, E. Fabbri, A. D'Epifanio, E. Di Bartolomeo, A. Tebano, S. Sanna, S. Licoccia, G. Balestrino and E. Traversa, *Nat. Mater.*, 9, 846–852 (2010).
43) S. H. Lee, K. I. Cho, J. B. Choi and D. W. Shin, *J. Power Sources*, 162, 1341–1345 (2006).
44) E. M. Rabinovich, M. I.-Shalom and A. Kisilev, *J. Mater. Sci.*, 15, 2027–2038 (1980).
45) J. O. Isard, *J. Non-Cryst. Solids*, 1, 235–261 (1969).
46) D. E. Day, *J. Non-Cryst. Solids*, 21, 343–372 (1976).
47) M. D. Ingram, *Phys. Chem. Glasses*, 28, 215–234 (1987).
48) Z. Shao and S. M. Halle, *Nature*, 431, 170–173 (2004).
49) Y. Daiko, T. Yamada, A. Mineshige and T. Yazawa, *2012 MRS fall symposium Proc.* (in press).
50) C. Wang, Y. Abe, T. Kasuga and M. Nogami, *J. Ceram. Soc. Japan*, 107, 1037–1040 (1999).

Yusuke Daiko received the Ph.D. at Nagoya Institute of Technology in 2006. From 2006 to 2008, he researched as a research fellow, Department of Materials Science, Toyohashi University of Technology, under the direction of Prof. A. Matsuda. From 2008 to 2013, he was employed as an Assistant Professor at the University of Hyogo. In 2013, he joined the Graduate School of Engineering, Nagoya Institute of Technology as an Assistant Professor.